Unformatted: Capacitive and memristive behaviours in metallic nanowire networks

C. O'Callaghan*,[1,2] C. G. Rocha,[1,2] F. Niosi,[3,2] H. G. Manning,[3,2] J. J. Boland,[3,2] and M. S. Ferreira[1,2]

[1]*School of Physics, Trinity College Dublin, Dublin 2, Ireland*

[2]*Centre for Research on Adaptive Nanostructures and Nanodevices (CRANN) & Advanced Materials and Bioengineering Research (AMBER) Centre, Trinity College Dublin, Dublin 2, Ireland*

[3]*School of Chemistry, Trinity College Dublin, Dublin 2, Ireland*

Abstract

Random nanowire networks (NWNs) are promising synthetic architectures for non-volatile memory devices and hardware-based neuromorphic applications due to their history-dependent responses, recurrent connectivity, and neurosynaptic-like behaviours. Such brain-like functions occur due to emergent resistive switching phenomena taking place in the interwire junctions which are viewed as memristive systems; they operate as smart analogue switches whose resistance depends on the history of the input voltage/current. We successfully demonstrated that NWNs made with a particular class of memristive junctions can exhibit a highly-selective conduction mechanism which uses the lowest-energy connectivity path in the network identified as the "winner-takes-all" state. The complex and adaptive behaviour of these junctions lead the system to channel the current through a single conductive path that spans the source-drain electrodes sandwiching the NWN. But these complex networks do not always behave in the same fashion; in the limit of sufficiently low input currents (preceding this selective conduction regime), the system behaves as a leakage capacitive network and its electrical activation is driven by cascades of breakdown-based switching events involving binary capacitive transitions. Understanding these two regimes is crucial to establish the potential of these materials for neuromorphics and for this we present two computational modelling schemes designed to describe the capacitive and memristive responses of NWNs interrogated adiabatically by voltage/current sources. In particular, our capacitive network model is regarded as a parallel RC circuit, with a leakage current term, to simulate their non-ideal capacitive properties. Our findings reveal the fault-tolerant aspect in the slow-switching dynamics of memristive networks in contrast with the abrupt activation response obtained in the fast-switching process of binary capacitive networks. Our results are corroborated by experimental evidence that reveal the fine electrical properties of NWN materials in their respective formation (capacitive) and conducting (memristive) stages.

I. INTRODUCTION

The study of network systems plays an important role in numerous scientific arenas (e.g. information technology, neurobiology, materials science, etc.) and provides valuable insights into a diverse range of complex phenomena that depend on their intricate connectivity patterns [1, 2]. Essentially any many-body system can be outlined as a network of nodes and edges and this includes large-scale grids such as the World-Wide Web as well as the smallest motifs in nature such as atoms arranged on a crystal lattice. A particular aspect of complex network systems is that the perfect knowledge of its individual parts will not necessarily lead to a perfect understanding of the whole system's behavior especially if its units are adaptable to changes in the environment [1, 3, 4]. Examples of complex adaptive networks are climate, ecosystems, financial markets, and perhaps the most fascinating of all, the human brain [5]. The latter is a highly complex machine formed by billions of neurons which are disorderly interconnected by trillions of synapses. Our brain has unique abilities that outperform by far the fastest computers on the planet such as ultra-fast sensory processing, high-level pattern recognition, and the ultimate skill of learning from experience. Brain activity is also incredibly energy-efficient; it consumes about 20 W, equivalent to a dim light bulb [6]. Such attributes have inspired the creation of the so-called neuromorphic (brain-like) devices that have the potential to revolutionize computing technology with the next-generation of microprocessors that will mimic brain functions[7–10].

To date, there has been numerous attempts to emulate brain-like processing using consolidated very-large-scale integration (VLSI) hardware[11]. It turns out that designing neuromorphic-based devices out of conventional CMOS technology can be extremely complex and expensive as a result of their rigid processing architecture combined with the characteristic von Neumann bottlenecks. Nonetheless, there are potentially cheaper and less complex platforms devised from a material science perspective that can be used as benchmarks for neuromorphic technologies. One of them consists of using smart synthetic materials composed of an entangled network of core-shell nanowires (NWs) that learn and adapt in response to external stimulation resembling in many aspects synapses of biological neural networks[12–14]. These networks typically consist of randomly dispersed metallic nanowires coated with an active dielectric shell from which new and intriguing electronic properties emerge; these materials are shown to behave as memristive (MR) systems in which their

electrical resistance depends on the history of the applied current or voltage drop[15, 16]. This is the key circuit ingredient that rules the learning process of these networks and their plasticity-like attributes.

Nanowire networks (NWNs) are promising MR architectures for neuromorphic applications due to their connectivity and neurosynaptic-like behaviours [12, 17, 18]. The latter takes place on the insulating layer coating intersecting wires in which a metal/insulator/metal (MIM) junction with MR properties is formed. A single MIM MR junction manifests complex non-equilibrium dynamics that are central for the neuromorphic capabilities of the whole network. The mechanism behind such dynamical behaviour is not unique and it depends on the material characteristics of the junction. Examples of MR materials [10] are transition metal oxides, amorphous-to-crystal phase materials such as GeSbTe, and polymeric matrices sandwiched by metals (e.g. Ag@PVP plates). During the breakdown of a MIM junction, the growth of a conducting filament (CF) bridging the metal plates takes place and this can be regulated by distinct mechanisms [16, 19–21] including thermochemical, electrochemical metallization, and valence change. With the filament gradual growth, a drastic reduction in the characteristic resistance of the junction can be measured.

In a recent work, we have reached unprecedented levels of control over the transport dynamics of NWNs in which we successfully set them to respond in a similar fashion as its fundamental units, the junctions [22]. Specifically, we demonstrated a self-similar scaling of the conductance of networks and the junctions that comprise them. We showed that this behaviour is an emergent property of a junction-dominated network that contains a particular class of junctions whose conductance grows supra-linearly with the injected current. These junctions enable the development of the so-called "winner-takes-all" (WTA) conducting path that spans the entire network, and which corresponds to the lowest-energy connectivity path [22, 23]. The full understanding of how WTA paths emerge provides unparalleled insights into the dynamics of electrically activated networks. However, the features of this activated regime is highly dependent on a precursor formation stage in which the network operates as a capacitor with almost no current flow. This regime is evident when the network is interrogated by sufficiently low currents (just a few pA); it characterizes a transient stage in which the entire NWN connectivity frame is electrically probed prior to selecting its least-resistance paths that will carry most of the current flow. Therefore, it is

crucial to understand (and to describe) not only the MR properties of NWN samples but also their capacitive features since these will practically define the most conductive regions of the network and its potential for WTA propagation.

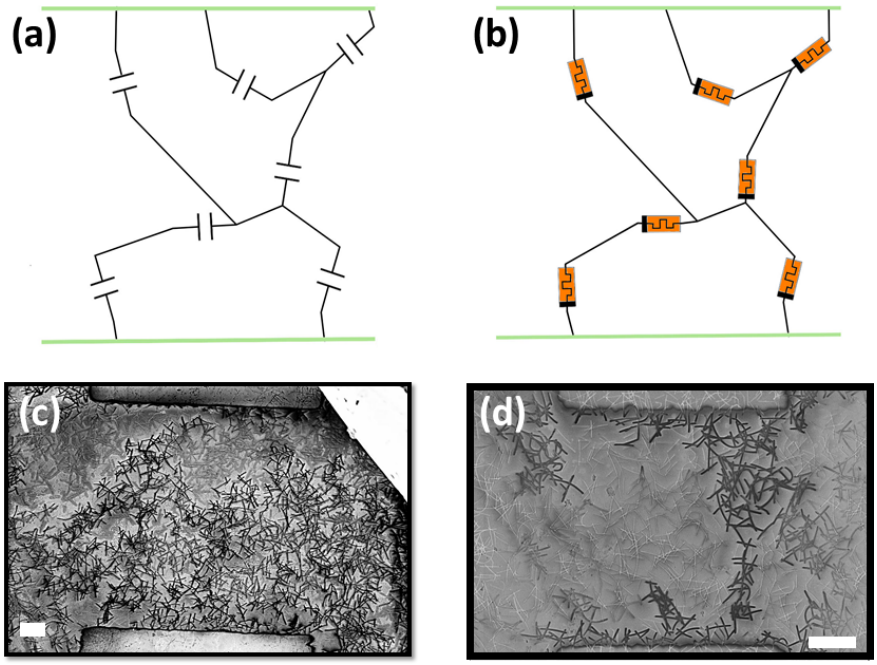

FIG. 1: (Top panels) Circuit sketches representing a NWN being described by a (a) capacitive model (CPM) and a (b) MR model (MRM). Each lumped circuit element is assigned to model the electrical characteristics of the interwire junctions in their respective formation (capacitors) and adaptive conducting (memristors) modes. Horizontal green lines represent metallic electrodes. (Bottom panels) PVC SEM images of Ag NWN samples subjected to distinct I-V characterizations. In (c), the image was taken by holding the source voltage at 2 Volts and setting a leakage current of few hundreds of pA. The network dimensions are 200 x 200 μm and the white scale bar corresponds to 20 μm. In (d), the image was taken from a full I-V sweep with a limiting current compliance of 500 nA. The network dimensions are 100 x 100 μm and the white scale bar corresponds to 2 μm. Darker wires are grounded to the electrodes meaning that their junctions were optimized in response to the given excitation. Almost the whole network is featured in the capacitive/formation regime whereas a single WTA path is contrasted in the memristive/conducting regime. More details on this experiment can be found in [22].

This work extends our knowledge on the development (and robustness) of conductive paths in complex NWNs by investigating their characteristic MR and capacitive behaviours. NWs connected by either capacitive or MR junctions are complementary models whose applicability depends on how the networks are interrogated. The capacitive response is dominant when the network is interrogated by extremely low currents ($\sim$ pA); in this regime, each junction is represented by a capacitor which breaks down if the voltage drop across it exceeds its characteristic threshold voltage. Once this occurs, the junction becomes a memristor at a high-resistance state (HRS) and sufficiently small currents can flow through it.

As more current is adiabatically sourced onto the network, the MR state of these junctions can be continuously evolved up to their respective low-resistance state (LRS). The outcomes of both capacitive and MR descriptions were systematically tracked and compared in this work by means of accurate multi-scale simulations. The results reveal great contrast in the dynamics of networks made of junctions that either have their state instantaneously flipped during dielectric breakdown (capacitive) or evolved continuously from HRS→LRS (memristive). These findings are consistent with direct observations of the electrical activation of the networks using passive voltage contrast (PVC) technique[24] (cf. Figure 1).

Our findings highlight the main differences between a breakdown-based switching process (involving binary capacitive transitions) and an gradual switch (involving analogue MR components) in complex NWN systems. NWNs made of slow-switching elements exhibit a continuous spectrum of conductance states bounded only by the junction cutoffs $\Gamma_{\text{off}} = 1/R_{\text{off}}$ and $\Gamma_{\text{on}} = 1/R_{\text{on}}$. This mechanism is shown to be highly selective, funnelling most of the sourced current through a single path (WTA state) of NWs bridging the electrodes. NWNs composed of fast-switching elements are not as selective however, with a much larger number of junctions playing an active role in forming a pathway between electrodes. We show that NWNs containing fast-switching elements evolve in a discrete fashion with the system alternating between stages of idleness and activity. While active, one can characterize the network dynamics by computing cascade events (or avalanches) comprised of clusters of junctions being activated simultaneously and their respective time durations. On the other hand, slow-switching junctions undergo a whole spectrum of conductance levels as the network is gradually excited by the current source. In this way, a binary cascade-like characterization cannot be conducted without the consideration of a (arbitrary) threshold parameter that classifies the occurrence (or not) of an avalanche event. Furthermore, we show that the slow-switching dynamics are fault-tolerant in response to perturbations, i.e. the network transport response is robust against junction failure. Only a minute increase in sheet conductance occurs at the moment a WTA path activation is slightly perturbed in the network. The fast-switching dynamics however are susceptible to larger-scale junction failures, requiring up to 55% additional switching events to form a continuously active pathway between electrodes.

II. COMPUTATIONAL METHODS

To illustrate the nonlinear mechanisms governing the formation and conduction processes in disordered NWNs, we developed two modelling schemes that will describe the network dynamics in the two distinctive regimes: a (i) fast-switching capacitive model (CPM) and a (ii) slow-switching MR model (MRM). Both models have already been used to capture the main dynamical features of numerous NWN samples and their outcomes are successfully supported by experimental data [22, 25, 26]. However, these models were never closely compared and, as we shall demonstrate, they will unveil distinct switching behaviours that play an important role in the synaptic-like response of electrically stressed NWNs.

All our NWNs are characterized by means of numerous I-V sweeps with a current limiting compliance being gradually ramped up during SET procedure. CPM accounts for the initial formation stage of the network in which it experiences residual amounts of input currents and all its interwire junctions are in their pristine insulating state. Therefore, in this scheme, the NWs are treated as equipotential wire segments and their connections as binary capacitors. Depending on the voltage drop across the capacitive junction, it can be either non-activated ($|0\rangle$) or activated ($|1\rangle$). The capacitance state of a junction can flip from $|0\rangle \rightarrow |1\rangle$ if the voltage drop across it is larger than its associated breakdown voltage (V_b), hence a given junction connecting a pair of wires (n, m) can be activated if $|V_n - V_m| \geq V_b$ where V_n (V_m) is the potential at wire n (m). The capacitor activation is characterized by a modification in the capacitance value of the junction as $C^0_{nm} \rightarrow C^1_{nm}$ where C^0_{nm} is an estimated quantity determined uniquely by the characteristics of the wires and $C^1_{nm} \rightarrow 0$ meaning that the junction has lost its capacitive properties and charge will start to flow through it. The values of C^0_{nm} are estimated by considering interwire junctions as parallel-plate capacitors with $C^0_{nm} = C^0 = \epsilon_r \epsilon_0 A/d \; \forall \; (n, m)$ pairs for the sake of simplicity. In the equation, ϵ_r is the relative permittivity of the dielectric, ϵ_0 is the permittivity of the air, A is the plate area, and d is the plate separation. For our PVP coated Ag NWs, we used $\epsilon_r \approx 2.5$, $d \approx 8$ nm and the area of the plates can be estimated from the NW diameters which range $D \sim 60-80$ nm. Assuming an ideal square area projected from two superimposed soft-body wires, $A = D^2$ and $C^0 \approx 18$ attoFarads (aF).

CPM simulation [25] begins by placing the whole capacitor network in contact with electrodes that source and drain a certain amount of charge Q, representing the charge

that builds up due to the applied bias voltage. The applied charge is incremented from an initial value Q_i up to a pre-defined maximum value of $Q_{\max}$ in steps of ΔQ. At Q_i, all junctions are set at $|0\rangle$-state and at each charge increment the electric potential of each wire is calculated and the potential difference across each junction is checked against the breakdown voltage. A capacitance matrix $\hat{M}_c$ is built taking into account the network connectivity and the potential on each wire is obtained by solving the system of equations $\hat{M}_c\hat{V} = \hat{Q}$ self-consistently. This means that charge on the electrodes is only incremented once all $|0\rangle \rightarrow |1\rangle$ transition activity on the network ceases.

As the input current applied on the network increases, one observes the NWN crossing over from a capacitive to an adaptive conducting regime which is better accounted by MRM. This is the stage in which most of the junctions in the NWN overcomes their initial formation state dominated by sufficiently large tunnel barriers. In other words, these probed junctions are now MRs and their transport mechanism is ruled by CF growth. As a result, the NWN begins to respond as a MR network in which it self-selects the most favourable routes for the current flow by means of least-resistance paths. We recently demonstrated that such controlled current-flow renders a self-similar scaling of the conductance of NWNs and the junctions that comprise them and this is the essence of the MRM [22]. It starts by relating conductance variation with the input current in single junctions, i.e. $\Gamma_j = f(I)$ where Γ_j is the conductance of the junction expressed as a function of the input current I. A "bottom-up" implementation approach is followed by incorporating the conductance law for individual junctions onto networks made by an interconnect of those elements. Measurements conducted in numerous junction systems including single interwire connections and individual wires of various core-shell materials (Ag@PVP, Ni@NiO, Ag@TiO_2, Cu@CuO, etc.) revealed that Γ_j scales with the current as a power law (PL),

$$\Gamma_j = A_j I^{\alpha_j} \tag{1}$$

where A_j is a proportionality constant and the exponent $\alpha_j \approx 1$. We demonstrated via ion-drift model analogy that these quantities are respectively related to the mobility of the diffusing charge-carriers in the junction and to the nonlinear effects caused by the strong electric fields present in the dielectric layer [22]. The resistance of junctions can vary continuously from a HRS ($R_{\text{off}} \sim 10^4$ kΩ) to a LRS that corresponds to the opening of a single conducting channel that bridges the metal plates. The conductance of this state is set to

be the quantum of conductance, $\Gamma_{\rm on} = 1/R_{\rm on} = 2e^2/h$ with e being the electron charge and h the Planck's constant. This junction model is then transferred to a NWN setting which includes junction resistance ($R_j = 1/\Gamma_j$) and inner wire resistance ($R_{\rm in}$) contributions interacting into a voltage-node network frame. While R_j characterizes a dynamical quantity in accordance to Eq. (1), R_{in} is fixed and it is given by $R_{in} = \rho\ell/S$ where ρ is the wire resistivity, ℓ is the wire segment length and S is the cross sectional area of the wire. These parameters were set to reported values for Ag@PVP NWs of $\rho = 22.6$ nΩm and wire diameters of 50 nm[27, 28]. The calculations involve iterating the amount of current sourced at the electrodes and at each current-step, the conductance of the entire network ($\Gamma_{\rm nt}$) is obtained numerically. Kirchhoff's circuit equations in matrix form $\hat{M}_\Gamma \hat{V} = \hat{I}$ are solved to calculate $\Gamma_{\rm nt}$ and to determine how the sourced current is distributed through the network [22]; $\hat{M}_\Gamma$ is the conductance matrix containing the network connectivity information and characteristic conductance values, $\hat{V}$ contains the potential at each node, and $\hat{I}$ contains the current injected/extracted at each electrode node. Therefore, the current flowing through an interwire junction connecting voltage nodes (n, m) can be obtained as

$$I_{n,m} = \frac{|V_n - V_m|}{R_j^{n,m}}. \tag{2}$$

For the first iteration, $R_j^{n,m} = R_{\rm off}\ \forall\ (n, m)$ internode pairs. Once $I_{n,m}$ is determined for all junctions, their new conductance state is obtained using the same functional form as in Eq. (1), i.e.

$$\Gamma_j^{n,m} = A_j (I_{n,m})^{\alpha_j}. \tag{3}$$

After updating the conductance of all junctions, the total current sourced on the electrodes is incremented and the whole procedure of calculating $\Gamma_j^{n,m}$ takes place recursively until the input current reaches a predefined maximum value of $I_{\rm max}$. The network conductance is then calculated for each sourced current value; such $\Gamma_{\rm nt} \times I$ curves are the main outcome of MRM.

For the sake of consistency, CPM and MRM were employed on the same NWN skeletons; although fundamentally different, both models are set to act on the same network geometries. Most of the simulations were parameterized for NWNs made of core-shell Ag@PVP NWs but our implementations are transferable to any material specification.

III. RESULTS

Figure 2(a) is an SEM image of one of our NWN sample made with Ag@PVP core-shell NWs. This NWN has a wire density of 0.47 NWs/μm^2 and the average length of the wires is about 7 μm. After conducting an image-processing procedure that recognizes the wire objects in the image and converts their pixel information onto a mathematical graph, we estimate that this network contains a total of 963 junctions. Figure 2(b) shows a stick representation of (a) which was built from the resultant graph [27]. By using an identical network geometry for both MRM and CPM simulations, the spatial fluctuations can be removed allowing a more direct comparison.

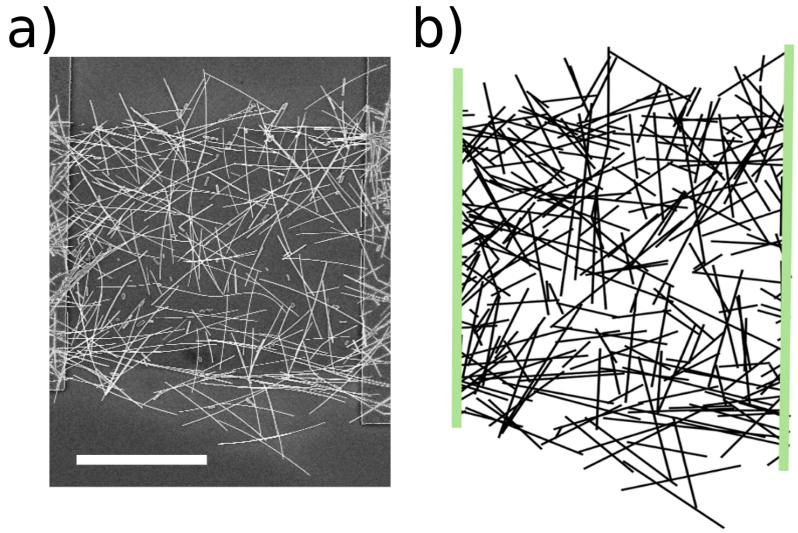

FIG. 2: (a) An SEM image of an Ag NWN with a wire density of 0.47 NWs/μm^2 and average wire length of 7μm. Electrodes are located at either sides of the network and the white scale bar at the bottom represents 10μm. (b) Stick representation of an Ag NWN sample taken from (a). Black sticks represent the Ag NWs whereas the vertical thick green lines represent the electrodes.

The network geometry shown in Figure 2 was first set to evolve in accordance to the MRM model from which $\Gamma_{\rm nt} \times I$ curves were obtained. The NWN is continuously driven through distinct conductive regimes and their characteristics depend on the properties of the junctions defined by Eq. (1) [22]. This can be seen in Figure 3 which depicts the evolution of the network conductance considering that its junctions follow a PL dynamics with $A_j = 0.05$ and $\alpha_j = 1.1$. These values are proven to describe with great success the MR dynamics of Ag@PVP NW junctions as evidenced by numerous experimental data [22]. Distinct conduction regimes are of note in Figure 3(a) being those (i) OFF-threshold (OFF),

(ii) transient growth (TG), (iii) power-law (PL), and (iv) post-power-law (PPL). The OFF-threshold region is the network ohmic response to low current levels. Here the current flowing through junctions is not high enough to cause a drastic change in conductance and we are going to demonstrate the capacitive properties of the network at this regime later on. At a certain critical current, the conductance of the network increases in a nonlinear fashion as junctions begin to improve their resistances (TG regime). Immediately after the TG region is the PL region where the junctions in the WTA path begin to evolve. Here there is a self-similarity between the collective network response and an individual junction response to increasing current compliance as both systems scale with the same exponent α_j [22]. This emergent phenomenon is due to the highly selective nature of current propagation for networks with $\alpha_j > 1$ in which practically all of the sourced current is channelled into the most energy-efficient conducting path, the WTA. At this state, the NWN responds as a unidimensional channel just as in a single junction. A visualisation of the activated wires at the end of the PL regime is shown in Figure 3(b). These activated wires are marked in black and they are found to carry most of the input current. This path contains 7 junctions evolving to the LRS meaning that just 0.72% of the junctions handle most of the current-flow workload in the PL regime. As more current is sourced onto the electrodes, other conducting paths are enabled in a discrete fashion. The device gradually acquires a two-dimensional character due to the formation of parallel conductive paths. About 80 supralinear junctions reach their optimum conductive state at $I = 30$ u.c. allowing the network to distribute the input current through multiple conducting paths. This is roughly 8.3% of the junctions taking part in the conduction process.

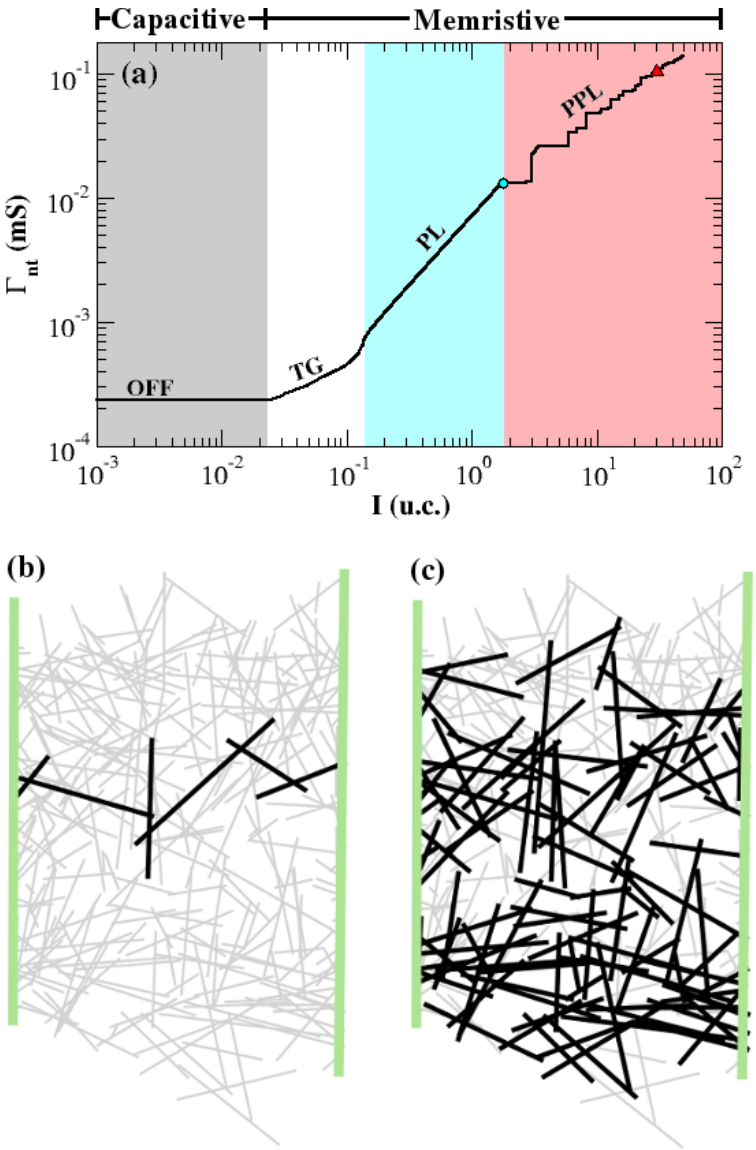

FIG. 3: (a) Simulated conductance versus current obtained for the image processed Ag NWN shown in Figure 2. The curve was taken MRM. All four distinct transport regimes discussed on the main text is depicted on panel and highlighted in different colours: (OFF) OFF-threshold, (TG) transient growth, (PL) power law, and (PPL) post-power-law. Currents are expressed in units of current (u.c.). The junction characteristics are set at $\alpha_j = 1.1$ and $A_j = 0.05$. The blue circle marks the point in the curve in which the junctions comprising the WTA paths are fully optimised at $I = 1.77$ u.c. and $\Gamma_{\rm nt} = 0.013$ mS. This point marks the disruption of the PL conducting regime. (b-c) NWN skeleton in which NWs connected by junctions at the LRS are highlighted in black and in light grey otherwise. The NWN snapshot depicted in (c) was taken at the PPL stage at $I = 30$ u.c..

At low current levels corresponding to the OFF-threshold in MRM, one can expect to find a capacitive response from the individual NW junctions coupled with some leakage current since their dielectric coating are not expected to be an ideal insulator; a small DC current can always leak through the dielectric material. To account for this dual response, CPM

is modified to incorporate leakage current in capacitive networks by considering a parallel RC circuit as a proxy for low current flow in NWNs. To simulate leakage currents of the order of pA, the resistance of this dummy resistor connected in parallel to the capacitive network (R_d) must be high enough, in this case we used $R_d \sim 10^{10}\,\Omega$. A potential difference that is placed across both elements then links the charge accumulated on the NWN with a leakage current through the resistor. Figure 4(a) is the gradual breakdown of a capacitive network by visualising the current flow required to cause an increasing charge build-up across the capacitor. One can identify a sudden increase in the required current flow at 6.22 aC. A visualisation of activated wires in the NWN at this point is presented in Figure 4 (b). Black wires represent those with an activated junction thus giving the wire an electrical connection with either of the electrodes. Junctions that are in contact or are near the electrodes activate easily as the potential difference builds quickest in these areas. Figure 4(c) shows the activated wires at the point when a continuous electrical path between the two electrodes has formed. The current levels through the resistor at this point is 1.3×10^{-7} A. A striking difference between both models can be seen here, the number of junctions that are activated before path formation in CPM is much greater than in path formation in MRM. In this case there are 61 junctions activated at path formation, i.e. 6.33% of junctions compared with 0.72% of junctions in the WTA path captured in MRM. Figure 4(d) is a visualisation of the network at a late stage of activation. Note the sudden jumps in the required leakage-current flow associated with clusters of breakdown events that are crucial for the development of the MR properties of the NWN during its adiabatic electrical stress. These jumps correspond to the sudden activation of wires in the network causing the effective capacitance of the network to drop suddenly. The current level through the resistor during capacitive activation is in the order of 10^{-7} A which compares favourably with current levels of hundreds of pA measured in the PVC image shown in Figure 1(c) and yet well below the current levels required for junction evolution in the MR regime.

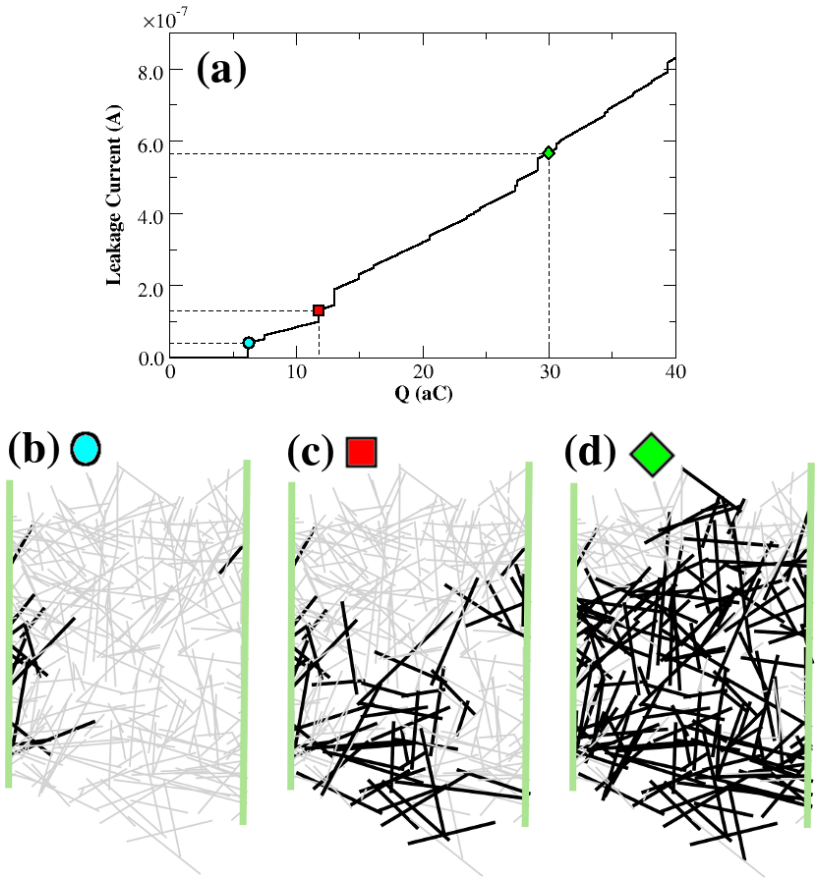

FIG. 4: (a) Leakage current through the parallel RC circuit as a function of the charge accumulation of the capacitive NWN. Steep jumps in current levels are clear at certain charge values and correspond to sudden activations of capacitive junctions. (b) Visualisation of the network at the first set of junction activations at 6.22 aC and leakage current of 4.2×10^{-8} A. Wires with an activated junction are in black and inactivated wires are in light grey. Figure (c) presents the activated wires when an electrical path between the electrodes is formed at 1.3×10^{-7} A and 11.78 aC. (d) Activated wires at a relatively high leakage current level at 5.7×10^{-7} A and 30 aC. Almost all junctions in the network underwent breakdown and the system is now MR at the HRS.

The sudden and large amount of junction activations, or avalanches, that give rise to the steps in leakage current flow offer much insight into the scale-free response of NWNs in the CPM approach. Of particular interest is the distribution in avalanche sizes and their respective relaxation times recorded during the CPM evolution (cf. Figure 5). The size of an avalanche (s) is defined as the number of junctions that break down at a given input charge Q. When at least one junction breaks down, the network self-organizes by redistributing its built-up charge throughout its remaining capacitive elements which can trigger subsequent avalanche events at the same charge input. The amount of iteration steps the network takes to relax its avalanche activity up to the point where $s = 0$ is defined as the avalanche lifetime or relaxation time (τ). Figure 5 shows the avalanche and lifetime distributions taken

for an ensemble containing 1000 Ag NWN samples of fixed wire density of 0.4 NWs/μm^2. The length of the wires is fixed at 7 μm and they are randomly spread over distinct device areas of 55 $\times$ 55, 60 $\times$ 60, and 70 $\times$ 70 μm. One can observe that both distributions depict a power-law trend which is indicative of scale-free critical behaviour in which a small perturbation can cause changes across the entire network. The exponents describing the avalanches and their respective lifetime statistics are rather close to the values found in a classic scale-free model, the 2D Abelian sandpile [29, 30]. As the network gets saturated with activations (the breakdown of a junction is assumed to be irreversible with $C^0_{nm} \leftarrow C^1_{nm}$ transitions being forbidden) the shape of the distributions is heavily affected by finite size effects caused by the closed boundaries of the device and the local constraints induced by the permanent capacitive properties of the junctions. Yet, we can say that NW meshes operating in the capacitive mode exhibit a collective integrated response to electrical stimuli that is independent of the device size, i.e. the emerging collective dynamics of capacitive NWN systems is scale-invariant at least within certain length/time scales.

In addition to the avalanche characterization provided by the computational model, we devised an experiment inspired by the works of Avizienis et al. [31] and Demis et al. [13] which evidences the collective dynamics of NWNs operating at leakage-current levels. The experiment consists of measuring time traces of leakage current in a NWN sample experiencing a DC bias voltage for a large period of time. By Fourier transforming the measured fluctuations in current, one can unveil complex emergent behaviours related to the activation process of the network and its recurrent connectivity structure. An Ag NWN of dimensions 1 $\times$ 1 mm was contacted through an Ag paste and electrical tests were performed using a Keithley 2400 source unit. We started by applying a bias voltage of 9.5 V but this was not sufficient to turn the network on. The bias was then increased to 10.5 V and the network current response was recorded for 20 hours in total. Only the first three hours of current data is required to analyse the leakage-current response of the sample because, after three hours of measurement, sufficiently high currents levels were recorded indicating that the network had surpassed leakage conduction. These results are shown in Figure 5(c-d). The presence of a power-law trend in the power spectrum points to a network-wide activation that is scale-free with a $1/f^\beta$ noise scaling with $\beta = 1.01$. As argued by Avizienis et al. [31], such persistent current fluctuations at DC bias indicate the capacity of the network in avoiding the formation of a single dominant high-conductivity pathway between electrodes.

This view agrees with the picture captured by our CPM (with a leakage term) of a scale-free clustering activation process in NWNs operating at a sufficiently low-current domain.

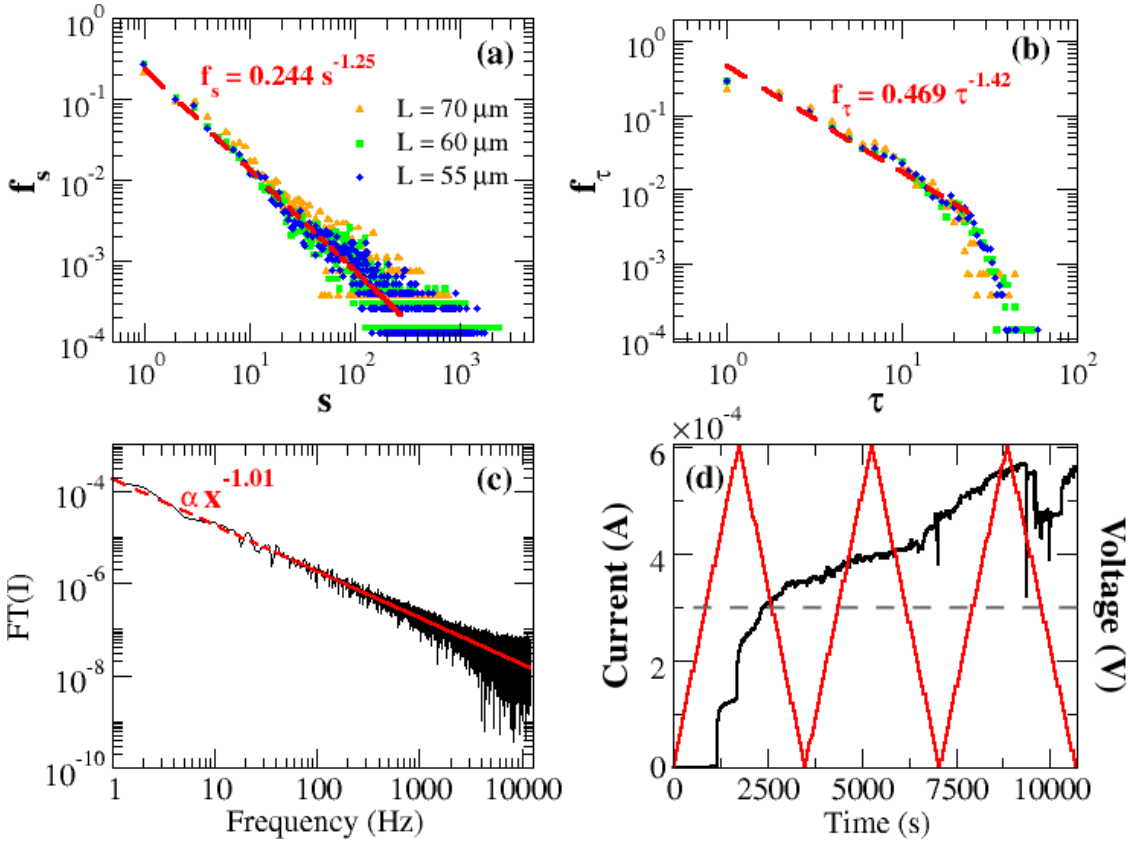

FIG. 5: (a) Avalanche (s) and its respective (b) lifetime (τ) frequency distributions in log-log scale taken for a random NWN ensemble containing over 1000 network samples of fixed wire density of 0.4 NWs/μm^2 and distinct sizes of 55 × 55, 60 × 60, and 70 × 70 μm. Note that for this result to acquire statistical significance, it needs to be taken for a large ensemble of random NWN samples rather than applying CPM onto the solely image-processed NWN sample of Figure 2. The dashed lines are power law fittings that give exponents of $\beta_s = -1.25$ for the avalanche distribution sizes and $\beta_\tau = -1.42$ for the lifetime distribution. Finite size effects play an important role in cutting off the power law trend specially in the lifetime results. (c) Fourier transform (in log-log scale) of the time traces of DC current response shown on panel (d). The power-law fit gives a $1/f^\beta$ scaling with an exponent $\beta = 1.01$. (d) Time traces of current response (black curve) to 10.5 V DC bias measured in an Ag NWN sample of dimensions 1 × 1 mm. The triangular bias sweep (red curve) shows the fine voltage range (10.4998 - 10.5002 V) around 10.5 V - marked by the dashed grey line - that the network experiences for almost three hours.

As so far demonstrated, disordered NWNs can exhibit scale-free capacitive activation or self-similar selective MR dynamics depending on which current range the network is being probed. In particular, such MR random networks are very attractive for probing collective features that are typical of biological neural systems such as adaptability, parallel processing, and fault-tolerance capabilities. Contrary to regular patterned devices - such as crossbar arrays [9, 32] - where each unit has a singular role, computation in random MR

networks relies on the non-deterministic action of their nonlinear elements distributed in a highly disordered manner. The disordered and dynamical natures of these networks make them ideal candidates to probe novel fault-tolerant computing paradigms. In other words, the massively parallel processing power characteristic of disordered interconnects combined with the adaptability of their building-blocks enables self-organization, reconfiguration, and self-healing to mitigate device shortcomings [33]. To illustrate such robustness to variability in random MR NWNs, we studied the role played by defects on their conduction response. A defect is made on a network composed of supralinear junctions exhibiting WTA conduction and it consists of removing a junction from this key path. This is a striking perturbation to consider since in principle it can destroy the current flow through the most favourite network path. MRM simulations were carried out to monitor the network conductance as a function of current for the defective system and compared with the original $\Gamma_{\mathrm{nt}} \times I$ curve shown in Figure 3(a). Figure 6(b) is a visualisation of the WTA path in the unperturbed network, identical to that shown in Figure 3(b). Figure 6(c) represents the new WTA path that is formed in the perturbed network with the destroyed junction represented by the red star. The conductance evolution for both original and defective NWN is almost identical at least until the first stages of the PPL regime as shown in Figure 6(c). The self-healing properties embedded in the dynamics of MR NWNs are clear in this example; the disruption of paths forces the junctions to re-adapt and this causes a redistribution of current across the network frame. The system then reconfigures into another least-resistance-path that does not aversely impact its overall conductance using hence just a little extra power to stress this second WTA path.

In the capacitive regime however we demonstrated that small perturbations can have a significant effect on the network dynamics as depicted in Figure 5(d-e). Here the network is perturbed by deleting a key junction that is involved in forming the path between electrodes in the CPM model. In Figure 6(d) the unperturbed network is presented when the leakage path between electrodes has been formed for the first time and this occurs at the charge of 11.77 aC. Figure 6(e) shows the activated wires at the moment of path formation for the perturbed network with one of its crucial junctions being destroyed from the start of the simulation (represented by the red star). This junction plays a pivotal role in the dynamics of path formation in the capacitive network which is evident when we compute the number of activated wires for both pristine and perturbed cases. The unperturbed network activates

61 wires whereas the defective one mobilizes 95 wires, an increase of 56% with respect to the benchmark pristine system. The charge required to form the electrode-electrode path also points to the sensitivity of the network to perturbations: 13.05 aC for the defective NWN compared with 11.77 aC for the unperturbed one. Contrasting the fault-tolerant results captured by CPM and MRM, one can conclude that the CPM shows a greater sensitivity to network geometry and connectivity profile and this sensitivity is manifested in the global capacitive properties of the network. The MRM however is much more robust; while the WTA path may completely re-route when a fault is encountered it does so in an efficient manner with little change in the global conductance of the network.

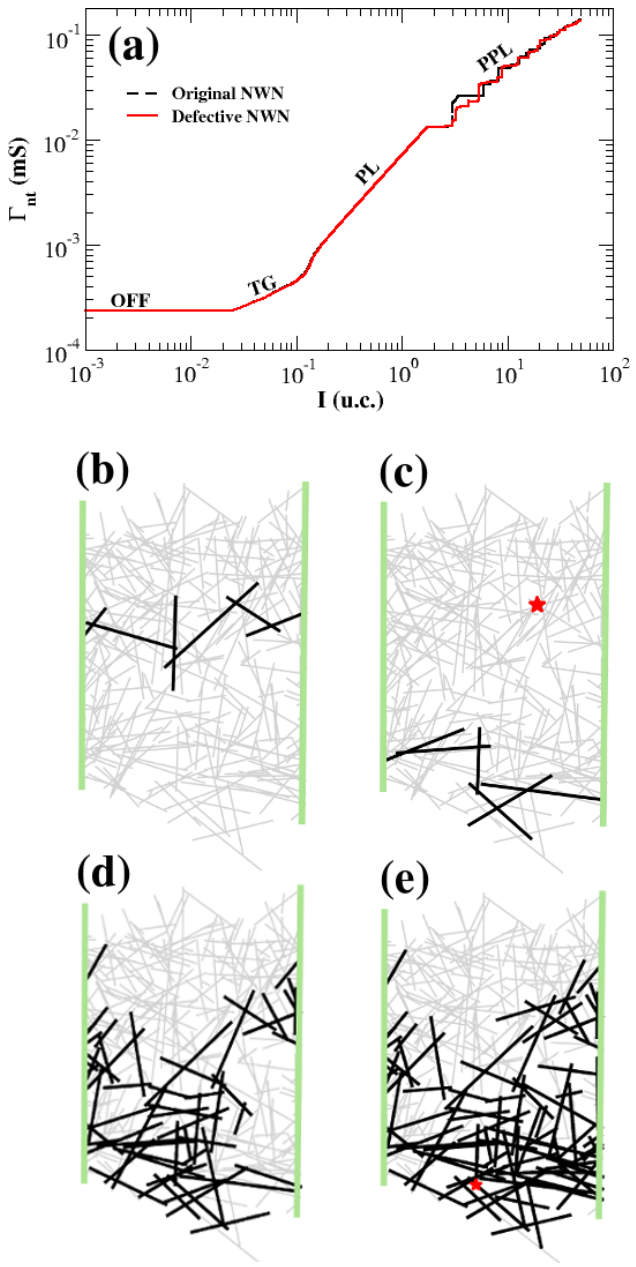

FIG. 6: (a) $\Gamma_{\rm nt} \times I$ curves obtained for the original (black dashed line) and the defective network (red line). The junction characteristics in these simulations are $\alpha_j = 1.1$ and $A_j = 0.05$. The curves only differ at the PPL regime. (b) Network diagram depicting wires in the WTA (black sticks) at $I = 1.77$ u.c. obtained using MRM in the original NWN. (c) A junction in this path was deleted and it is highlighted by a red star symbol. The network self-organizes the current transmission to another WTA path located at its bottom part. This path contains the same amount of junctions as in the original network, i.e. 7 junctions. Wires carrying residual or no current at all appear in light grey. Vertical green lines represent the electrodes that source current onto the network. (d) Network diagram depicting activated wires (black sticks) in the original NWN described as a capacitive system via CPM. (e) The same activation simulation as in (d) but with a defective junction marked with a red star symbol. One can clearly notice, by comparing panels (b)↔(d) and (c)↔(e), the selective↔clustering activation of the NWN treated as an analog MR model (MRM) or as a binary capacitive model (CPM). This contrasting feature is also captured experimentally in Figure 1(c-d).

IV. CONCLUSION

In this work, we presented two computational methods designed to describe the electrical and conduction properties of random NWNs made of core-shell NWs interrogated by voltage/current sources. The methods successfully model the leakage capacitive (CPM) and memristive (MRM) responses of NWNs perturbed at distinct transport regimes. The network is shown to behave as a leakage capacitor when sufficiently low currents ($\sim$ pA) are applied onto the system. CPM is then used to emulate a cascade of breakdown-based switching events characterized by pristine dielectric junctions in the network loosing their capacitive properties when the voltage drop across them exceeds a characteristic threshold voltage. In turn, these junctions are recast as a MR unit - initially at a HRS - which can be continuously evolved up to their respective LRS as more current is adiabatically sourced onto the network. Such MR dynamics in networks is outlined with the MRM which makes use of an empirical power-law functional to describe the HRS$\rightarrow$LRS evolution of the junctions. The two descriptions reveal the highly contrasting dynamics exhibited by the NWN responding as a capacitive or a MR system. Networks in the capacitive regime undergo a long-range activation process with clusters of capacitive junctions being activated in a binary fashion. This causes the current to "leak" through the network in a discrete manner as a result of the abrupt collective activation of junction groups. We demonstrated that this dynamics manifests complex emergent behaviours such as spatially correlated activation and scale-invariant avalanche distributions. As the capacitive properties of the network fade in response to the increase of input current, its MR dynamics takes over and the slow-switching feature of the MR junctions starts to play a role. This gives rise to a highly-selective conduction mechanism in which the NWN junctions reconfigure their resistive state to channel most of the current-flow to the WTA path. The latter consists of an emergent internal state that uses minimum power by transmitting the sourced current through the least-resistance path rather than spreading into multiple current-carrying paths across the network. This conduction regime is better described by the MRM which further reveals other emergent characteristics of complex networks with adaptive/reconfigurable elements such as self-similarity, multi-level conductance switching, and fault-tolerance capabilities. Our results are supported by striking experimental evidences that unfold the recurrent dynamics of the networks via direct observation of PVC images and power spectrum analysis of

their temporal DC response. Our findings show that random NWNs are complex synthetic materials that span a rich range of emergent properties and conduction mechanisms that can be employed in brain-like computing ranging from logics (suitable in the capacitive regime) to analog processing (fit for the MR regime).

---

[1] S. H. Strogatz, Nature **410**, 268 (2001).

[2] M. E. J. Newman, SIAM Rev. **45**, 167 (2003).

[3] B. J. West, M. Turalska, and P. Grigolini, New Journal of Physics **17**, 045009 (2015).

[4] G. Chen, X. Wang, and X. Li, *Fundamentals of complex networks: models, structures and dynamics* (John Wiley & Sons, 2015).

[5] I. J. G. Portillo and P. M. Gleiser, PLoS One **4**, e6863 (2009).

[6] B. Sengupta and M. B. Stemmler, Proc. IEEE **102**, 738 (2014).

[7] C. Mead, Proc. IEEE **78**, 1629 (1990).

[8] A. Calimera, E. Macii, and M. Poncino, Functional Neurology **28**, 191 (2013).

[9] M. Prezioso, F. Merrikh-Bayat, B. D. Hoskins, G. C. Adam, K. K. Likharev, and D. B. Strukov, Nature **521**, 61 (2015).

[10] J. J. Yang, D. B. Strukov, and D. R. Stewart, Nature Nanotechnology **8**, 13 (2013).

[11] G. Indiveri, B. Linares-Barranco, R. Legenstein, G. Deligeorgis, and T. Prodromakis, Nanotechnology **24**, 384010 (2013).

[12] P. N. Nirmalraj, A. T. Bellew, A. P. Bell, J. A. Fairfield, E. K. McCarthy, C. J. O'Kelly, L. F. C. Pereira, S. Sorel, D. Morosan, J. N. Coleman, et al., Nano Lett. **12**, 5966 (2012).

[13] E. C. Demis, R. Aguilera, K. Scharnhorst, M. Aono, A. Z. Stieg, and J. K. Gimzewski, Japanese Journal of Applied Physics **55**, 1102B2 (2016).

[14] H. O. Sillin, R. Aguilera, H.-H. Shieh, A. V. Avizienis, M. Aono, A. Z. Stieg, and J. K. Gimzewski, Nanotechnology **24**, 384004 (2013).

[15] L. Chua, IEEE Trans. Circuit Theory **18**, 507 (1971).

[16] R. Tetzlaff, ed., *Memristors and memristive systems* (Springer-Verlag New York, 2014).

[17] C. J. O'Kelly, J. A. Fairfield, D. McCloskey, H. G. Manning, J. F. Donegan, and J. J. Boland, Advanced Electronic Materials **2**, 1500458 (2016).

[18] S. H. Jo, T. Chang, I. Ebong, B. B. Bhadviya, P. Mazumder, and W. Lu, Nano Lett. **10**, 1297

(2010).

[19] E. W. Lim and R. Ismail, Electronics **4**, 586 (2015).

[20] D. S. Jeong, R. Thomas, R. Katiyar, J. Scott, H. Kohlstedt, A. Petraru, and C. S. Hwang, Reports on Progress in Physics **75**, 076502 (2012).

[21] H. G. Manning, S. Biswas, J. D. Holmes, and J. J. Boland, ACS Applied Materials & Interfaces **9**, 38959 (2017).

[22] H. G. Manning, F. Niosi, C. G. Rocha, C. O'Callaghan, A. T. Bellew, S. Biswas, P. Flowers, B. J. Wiley, J. T. Holmes, M. S. Ferreira, et al., To appear (2017).

[23] U. Celano, G. Giammaria, L. Goux, A. Belmonte, M. Jurczak, and W. Vandervorst, Nanoscale **8**, 13915 (2016).

[24] Z. Gemmill, L. Durbha, S. Jacobson, G. Gao, and K. Weaver, Microelectronic Failure Analysis Desk Reference, 5th edn. pp. 431–437 (2004).

[25] J. A. Fairfield, C. G. Rocha, C. O'Callaghan, M. S. Ferreira, and J. J. Boland, Nanoscale **8**, 18516 (2016).

[26] A. T. Bellew, H. G. Manning, C. G. Rocha, M. S. Ferreira, and J. J. Boland, ACS Nano **9**, 11422 (2015).

[27] C. G. Rocha, H. G. Manning, C. O'Callaghan, C. Ritter, A. T. Bellew, J. J. Boland, and M. S. Ferreira, Nanoscale **7**, 13011 (2015).

[28] C. O'Callaghan, C. G. Rocha, H. G. Manning, J. J. Boland, and M. S. Ferreira, Physical Chemistry Chemical Physics **18**, 27564 (2016).

[29] L. Pietronero, A. Vespignani, and S. Zapperi, Physical Review Letters **72**, 1690 (1994).

[30] V. B. Priezzhev, D. V. Ktitarev, and E. V. Ivashkevich, Physical Review Letters **76**, 2093 (1996).

[31] A. V. Avizienis, H. O. Sillin, C. Martin-Olmos, H. H. Shieh, M. Aono, A. Z. Stieg, and J. K. Gimzewski, PLoS One **7**, e42772 (2012).

[32] K.-H. Kim, S. Gaba, D. Wheeler, J. M. Cruz-Albrecht, T. Hussain, N. Srinivasa, and W. Lu, Nano Lett. **12**, 389 (2012).

[33] G. S. Snider, Nanotechnology **18**, 365202 (2007).